Environmental Science & Technology

Article

Cite This: Environ. Sci. Technol. 2019, 53, 10665−10675

pubs.acs.org/est

Climate and Vegetation As Primary Drivers for Global Mercury Storage in Surface Soil

Xun Wang,[†] Wei Yuan,[†,‡] Che-Jen Lin,[⊥,§] Leiming Zhang,[∥] Hui Zhang,[†] and Xinbin Feng*[,†,#]

[†]State Key Laboratory of Environmental Geochemistry, Institute of Geochemistry, Chinese Academy of Sciences, Guiyang 550081, China

[‡]University of Chinese Academy of Sciences, Beijing 100049, China

[⊥]Center for Advances in Water and Air Quality, Lamar University, Beaumont, Texas 77705, United States

[§]Department of Civil and Environmental Engineering, Lamar University, Beaumont, Texas 77705, United States

[∥]Air Quality Research Division, Science and Technology Branch, Environment and Climate Change Canada, Toronto, Ontario M3H 5T4, Canada

[#]Center for Excellence in Quaternary Science and Global Change, Chinese Academy of Sciences, Xian 710061, China

Supporting Information

ABSTRACT: Soil is the largest Hg reservoir globally. Data of Hg concentration in surface soil are fundamental to understanding environmental Hg cycling. However, present knowledge on the quantity and global distribution of Hg in soil remains deficient. Using stable Hg isotopic analyses and geospatial data, the concentration and global spatial distribution of Hg in surface soil of 0−20 cm depth have been developed. It is estimated that 1088 ± 379 Gg of Hg is stored in surface soil globally. Thirty-two percent of the surface Hg storage resides in tropical/subtropical forest regions, 23% in temperate/boreal forest regions, 28% in grassland and steppe and shrubland, 7% in tundra, and 10% in desert and xeric shrubland. Evidence from Hg isotopic signatures points to atmospheric Hg^0 dry deposition through vegetation uptake as the primary source of Hg in surface soil. Given the influence of changing climate on vegetative development, global climate change can act as an important forcing factor for shaping spatial distribution of Hg in surface soil. This active forcing cycle significantly dilutes the impacts caused by Hg release from anthropogenic sources, and needs to be considered in assessing the effectiveness of reducing Hg use and emissions as specified in *Minamata Convention on Mercury*.

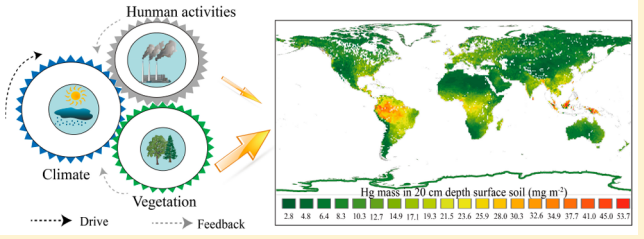

1. INTRODUCTION

The ratification of *Minamata Convention on Mercury* (Hg) in 2017 is widely considered a success to protect human health and the environment from the detrimental effects of Hg.[1] However, existing Hg data and scientific knowledge are insufficient to adequately assess the policy benefits in reducing human and wildlife Hg exposure.[2] To date, the spatial distribution of Hg concentration in soils across the globe remains largely uncertain.[3,4] Earlier studies reported 235−1150 Gg of Hg storage in surface soil across the globe.[3,5−8] Such a data set is critical for a complete understanding of Hg cycling. Uncertainties in soil Hg data limit our ability to quantify legacy Hg emission from soil to the atmosphere,[2] estimating Hg runoff from uplands to the aquatic environment,[9] and assessing potential risks of human and wildlife Hg exposure globally.[10]

The concentration and distribution of soil Hg are best estimated with representative soil samples collected in a global observational network, but such an approach is not feasible because of the limitation of access and cost to perform such a global study. Statistic regression modeling (e.g., multiple linear regression) using the large geological database provides another alternative for reliably constructing global concentration and distribution of Hg in soil. Using available data of Hg concentration and distribution in China and the U.S.,[11−13] coupled with global organic carbon, meteorological factors, and anthropogenic Hg emissions data sets, it is possible to gain insight on the contributing sources and accumulation pathways of Hg in soil at a global scale.

The sources of Hg in surface soil are from atmospheric deposition of elemental Hg (Hg^0) (i.e., atmospheric Hg^0 uptake by vegetation and input to soil with plant detritus) and oxidized Hg (Hg^{2+}),[9,14,15] and from weathering of Hg from rocks.[9,14,16] Runoff-related accumulation from contaminated waters is likely an important source in areas that have received air emission or water discharge of Hg from human activities,[4,17] which is largely localized near anthropogenic sources. Since direct or standardized quantification methods

Received: April 19, 2019
Revised: July 17, 2019
Accepted: July 20, 2019
Published: August 21, 2019

DOI: 10.1021/acs.est.9b02386
Environ. Sci. Technol. 2019, 53, 10665−10675

for measuring Hg dry deposition is not available, Hg dry deposition is often estimated by models, or by surrogate measurements such as Hg deposition through litterfall or on artificial surfaces.[15] Mercury wet deposition has been the primary focus in quantifying Hg input to terrestrial and aquatic ecosystems. Networks of Hg wet deposition measurement have been established globally, such as Global Mercury Observation System (GMOS)[18] and National Atmospheric Deposition Program's (NADP) Mercury Deposition Network (MDN) sites in North America.[15] However, recent studies have highlighted the importance of Hg dry deposition to the terrestrial ecosystem. Specifically, atmospheric Hg^0 uptake by vegetation is responsible for substantial Hg accumulation in forest ecosystems,[14,19−22] as well as for the observed seasonal variation of atmospheric Hg concentrations.[23,24] Climate is the main driver for vegetation distribution globally.[25−28] The atmospheric Hg^0 dry deposition through vegetation uptake whose spatial distribution is driven by vegetative development[29,30] is closely tied to the changing climate. Therefore, global climate change is an important forcing factor for shaping spatial distribution of Hg in surface soil. Time profiles of Hg deposition reconstructed from lake sediments and peat bogs have demonstrated that the changes of climate and vegetation coverage as well as related forest fire paleo-history are the main drivers for the natural changes in Hg deposition flux and subsequent concentrations in terrestrial ecosystems.[31−33]

Recent advancement of stable Hg isotope techniques enables delineation of the origins and accumulation processes of Hg in surface soil. Mercury undergoes both mass dependent fractionation (MDF, reported as δ^{202}Hg) and mass independent fractionation (MIF, reported as Δ^{199}Hg, Δ^{200}Hg, and Δ^{201}Hg) in the environment.[16] The MIF signatures of Hg isotopes are much less likely to be altered by postdepositional processes than MDF in the environment, making the MIF signatures of Hg useful tracers for identifying different sources.[14,16,34] Atmospheric Hg^{2+} is characterized by positive Δ^{199}Hg, Δ^{200}Hg, and Δ^{201}Hg values, whereas Hg^0 in the atmosphere shows negative values of Δ^{199}Hg and Δ^{201}Hg with negligible Δ^{200}Hg.[14,16,34] Geological Hg pool exhibits zero Δ^{199}Hg, Δ^{200}Hg, and Δ^{201}Hg.[14,16,34]

We hypothesized that the active processes driven by climate and vegetative development influence soil Hg spatial distribution at continental and global scales. This study focuses on atmospheric Hg^0 deposition forced by climate and vegetative development, as well as its effect on soil Hg spatial distribution at a global scale. Comprehensive data of Hg isotopic signatures measured in global terrestrial ecosystems are analyzed, coupled with structural equation modeling using geospatial data sets collected in China and the U.S., to verify the hypothesis. Based on the analysis, global spatial distribution of Hg in the top 0−20 cm of surface soil (consisting of organic soil and upper mineral soil in terrestrial ecosystems) is constructed. The implications of the soil Hg storage on global Hg cycling under climate change scenarios are discussed.

2. MATERIALS AND METHODS

2.1. Sites Description, Sampling, and Measurements. Hg concentration and isotopic composition in vegetation and soil samples were measured at 13 agricultural land sites, 26 forest sites, 11 grassland sites, and 2 Tibetan wetland sites across China (Supporting Information (SI) Figure S1). The samples, collected from 2014 to 2018, include tree foliage, litterfall, grass, and straw, and soil at 0−20 and 100 cm depth. The site information is provided in SI Table S1. The sampling protocol has been described in detail in our earlier studies.[14] Briefly, five 5 × 5 m subplots at each site were established for sample collection, and each ∼500 g of samples for well mixed vegetation, 0−20 cm surface soils, and 100 cm deep soils were collected. Yang et al.[35] suggested that vegetation samples freeze-dried or oven-dried at <65 °C were suitable for determination of Hg. Vegetation samples were dried in an oven at 60 °C for 48 h until <0.03% of mass variation occurred in 8 h and ground by a separate electric grinder. Soil samples were air-dried in a dark and clean room and ground in an agate mortar and sieved by a 200 mesh sieve (74 μm). In addition, data from 15 documented forest sites, 4 tundra sites, and 1 peatland site across the globe[19,21,22,36−39] were reviewed and analyzed to understand soil Hg sources in these ecosystems. We have reported surface soil Hg isotopic compositions at 10 cm depth of 23 Tibetan forest sites.[14] In this study, we reported Hg isotopic compositions in surface soil at 20 cm depth for these sites. We found that δ^{202}Hg and Δ^{199}Hg in soil at 0−20 cm depth of these sites were slightly positive than values at soil 0−10 cm depth (∼0.02−0.10‰ shift for δ^{202}Hg, and 0.04−0.10‰ shift for Δ^{199}Hg, $p > 0.05$, by paired-t test).

The procedure for Hg isotope measurement of vegetation and soil samples has been described in our earlier work[14] (detailed in the SI). Mercury isotopic compositions are measured using the standard-sample-standard (SPS) protocol. The HgMDF is reported in δ notation using the unit of permil (‰) referenced to the neighboring NIST-3133 solution:

$$\delta^{202}\mathrm{Hg}(‰) = 1000 \times [(^{202}\mathrm{Hg}/^{198}\mathrm{Hg}_{\mathrm{sample}}) / (^{202}\mathrm{Hg}/^{198}\mathrm{Hg}_{\mathrm{NISTSRM3133}}) - 1] \quad (1)$$

The MIF is reported as Δ^{xxx}Hg following the convention suggested by Blum and Bergquist:[40]

$$\Delta^{199}\mathrm{Hg}(‰) = \delta^{199}\mathrm{Hg} - 0.2520 \times \delta^{202}\mathrm{Hg} \quad (2)$$

$$\Delta^{200}\mathrm{Hg}(‰) = \delta^{200}\mathrm{Hg} - 0.5024 \times \delta^{202}\mathrm{Hg} \quad (3)$$

$$\Delta^{201}\mathrm{Hg}(‰) = \delta^{201}\mathrm{Hg} - 0.7520 \times \delta^{202}\mathrm{Hg} \quad (4)$$

UM-Almadén secondary standard was analyzed every 10 samples. The results of UM-Almadén are consistent with reported values (δ^{202}Hg = −0.53 ± 0.04‰, Δ^{199}Hg = −0.01 ± 0.04‰, Δ^{201}Hg = −0.01 ± 0.05‰, Δ^{200}Hg = 0.01 ± 0.03‰, n = 13) and BCR-482 (δ^{202}Hg = −1.56 ± 0.06‰, Δ^{199}Hg = −0.63 ± 0.02‰, Δ^{201}Hg = −0.63 ± 0.02‰, Δ^{200}Hg = 0.03 ± 0.03‰, n = 4) and GSS-4 (δ^{202}Hg = −1.72 ± 0.08‰, Δ^{199}Hg = −0.34 ± 0.03‰, Δ^{201}Hg = −0.34 ± 0.03‰, Δ^{200}Hg = −0.00 ± 0.02‰, mean ±1 SD, n = 4).[40,41]

2.2. Mapping of Global Surface Soil Hg Concentration. The data collection and availability are described in the SI. Given the diverse spatial and temporal scales of these data sets, all data were regridded into a 1° × 1° grid cell. The volume of data set for 0−20 cm surface soil Hg concentration in China (about 50 000 points) is much larger than the volume of data set in the U.S. (about 2000 points) in this study. To ensure data comparability, the grid cell in the U.S. with less than three data points of surface soil Hg concentration was not considered. Similarly, the data sets of climate and vegetation factors, population distribution, and anthropogenic Hg emission were regridded into the same resolution of 1° × 1°. Then, structural equation modeling and regression analyses

DOI: 10.1021/acs.est.9b02386
Environ. Sci. Technol. 2019, 53, 10665−10675

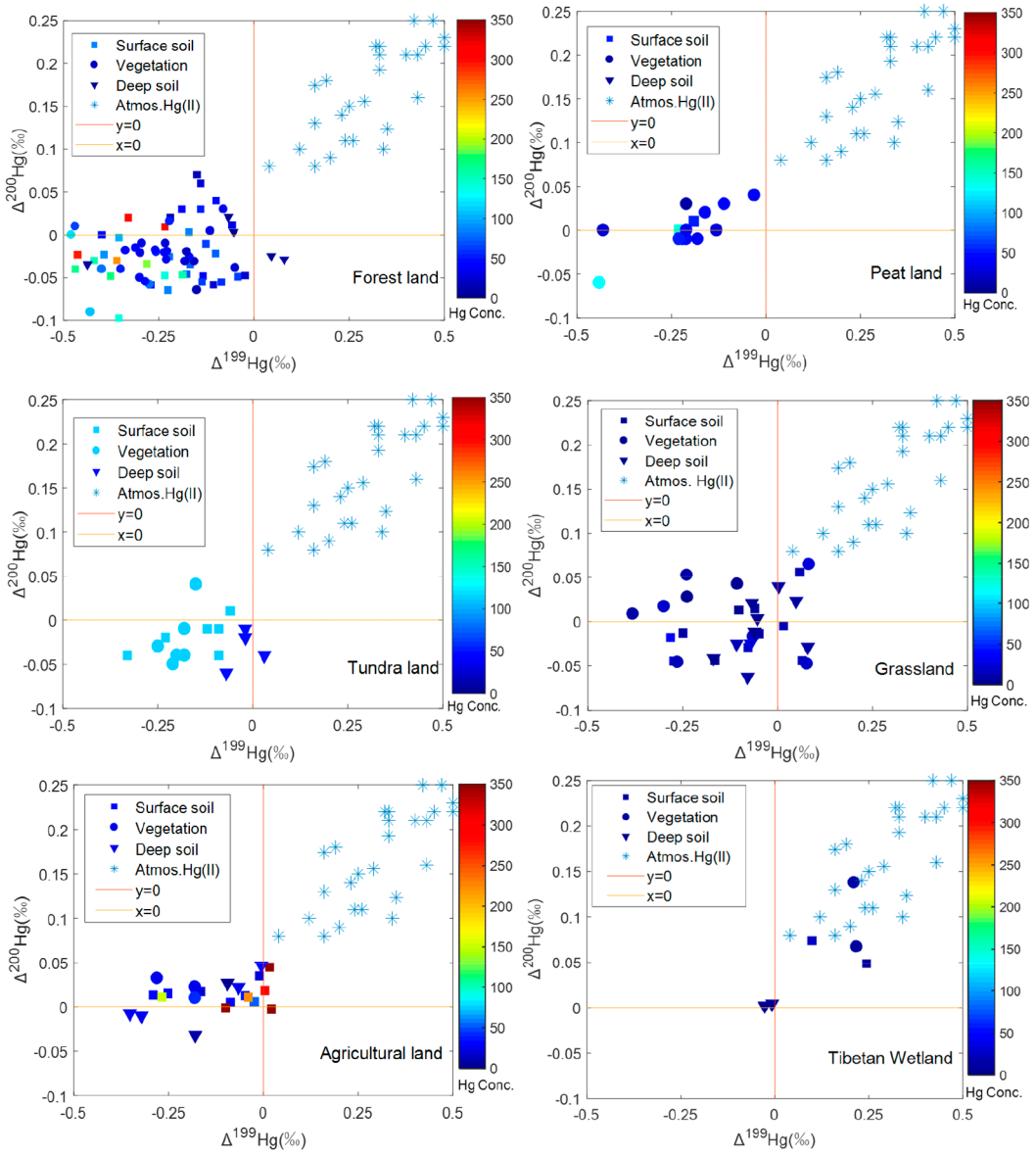

Figure 1. Hg MIF signatures in agricultural-land, forest-land, grass-land, peat-land, tundra-land, and Tibetan wetland. The Hg isotopic signatures for atmospheric Hg^{2+} are derived from the literature.[37,39,84−87] The surface soil is 0−20 cm soil or top A soil, and the deep soil is 100 cm soil. The Hg concentration is in the unit of ng g^{-1}. We used average Hg isotopic signatures at each site for earlier reported values.[19,21,22,36−39]

were processed by Amos 21 and SPSS 16. ArcGIS 10.4 was utilized to create the global map of Hg concentration in surface soil. The global 0−20 cm surface soil Hg storage (HgP) is estimated as

$$\mathrm{HgP} = \mathrm{HgC} \times \mathrm{BD} \times (1 - f) \times 20 \quad (5)$$

where HgC is soil Hg concentration, BD is the soil bulk density, and f is the soil coarse fragments (>2 mm) volume in 0−20 cm surface soil. Given the climate, vegetation, and human influences (details in Results and Discussion), we used MLR (multiple linear regression) to obtain the empirical model to predict the global surface soil Hg concentration as follows:

$$\log(\mathrm{HgC}_1) = -12.893 + 0.551\log(P) + 7.651\log(T) - 0.085\log(\mathrm{NPP}) - 1.366\log(R) + 0.029\log(\mathrm{Hg}^{2+}) + 0.357 \times \log(\mathrm{SOC}),\ R^2 = 0.57,\ P < 0.01 \quad (6)$$

where HgC_1 is the 0−20 cm surface soil Hg concentration (ng g^{-1}, induced by climate, vegetation, and human influences), P is precipitation (mm), T is air temperature (K), NPP is net primary production (g m^{-2} day^{-1}), R is solar radiation (w m^{-2}), Hg^{2+} is anthropogenic Hg^{2+}emission (g km^{-2}), and SOC is soil organic carbon (%). All data in eq 6 are from the 1° × 1° grid cell in China and the U.S. (SI Figure S2).The anthropogenic Hg emission inventory is from AMAP/UNEP 2010.[42] The eq 6 did not consider the difference caused by potential influence of geological Hg sources since its intercept is ∼0 (i.e., $10^{-12.893}$). Earlier studies suggested that crustal Hg typically exists at low concentration with small variations (except in Hg-enriched zone) and its contribution to the vegetative surface soil is insignificant. For example, crustal Hg concentration varies from 7 to 24 ng g^{-1} (average = 11 ng g^{-1}) in China,[11] and has an average of 10 ng g^{-1} in parent soil of U.S.[13] In Australia, 50% of Hg concentration in 60−80 cm soil is less than 10 ng g^{-1} (n = 1314).[43] Thus, we applied a level of

DOI: 10.1021/acs.est.9b02386
Environ. Sci. Technol. 2019, 53, 10665−10675

10 ng g^{-1} Hg concentration in geological sources. It was found that the geological source fraction (f_{geo}) in 0−20 cm surface soil was best estimated by SOC (details of Hg isotope mixing model in SI) as

$$f_{geo} = -0.154\ln(SOC) + 0.5311R^2 = 0.58,\ P < 0.01,\ n = 41 \quad (7)$$

Incorporating the contribution from geologic source, HgC in eq 5 can be modified as

$$HgC = HgC_1 + 10 \times f_{geo} \quad (8)$$

HgC is set to 10 ng g^{-1} if HgC is less than 10 ng g^{-1} because of the surface soil Hg concentration at least greater than the crustal Hg except for in Hg-enriched zone.

2.3. Statistical Methods. In this study, all China and U.S. data including climate, biotic, anthropogenic, and edaphic characteristics were subject to logarithmic transformation to meet the assumptions of normality. We used the bivariate Pearson Correlation to produce the correlation coefficient among factors of climate, anthropogenic influences, vegetation, and soil Hg concentration at 95% confidence interval by two-tailed test. Based on the correlation analysis, we further used conceptual structural equation modeling to construct the impacts from climate, anthropogenic influences, vegetation on soil Hg spatial distribution. It is noteworthy that we used principal component analyses (PCAs) to create multivariate functional indexes to represent the individual impact from climate, vegetation, and anthropogenic activities (details in Section 3.2). All indexes were then standardized into Z-scores. Finally, structural equation modeling was developed from the conceptual model using χ^2 tests with maximum likelihood estimation. Model fitting was performed by using SPSS version 17 and the Amos software version 24. We used p-values (at least >0.05), χ^2 values, and degree of freedom (df) as the criteria for evaluation of structural equation modeling fit. From the structural equation modeling path network, the standardized path coefficient (β, i.e., a value closer to 1 represents a stronger influence) represents the direct effect of one variable on another, and the indirect effect (e.g., one variable affects another variable which in turn affects a third) is calculated by multiplying each associated β.

3. RESULTS AND DISCUSSION

3.1. Climate and Vegetation Influences Revealed by Hg Isotopic Signatures. Atmospheric Hg^0 uptake has been suggested to be the primary source of Hg in foliage of forest, cropland, peatland, and tundra ecosystems.[14,15,36,37] Lighter Hg isotopes in air are preferentially accumulated in the foliage, causing a −3.0‰ to −1‰ δ^{202}Hg shift between air and foliage.[16,34,36] Combining our field sites in China and the referenced sites (SI Tables S1 and S2), significantly more negative δ^{202}Hg values are observed in tree foliage samples (−2.77 ± 0.39‰, Mean ±1 SD, n = 28 sites, SI Table S1) compared to the values for grass and straw biomass samples (−1.52 ± 0.31‰, n = 30 sites) ($p < 0.001$, by t test) at rural sites. This difference may be explained by the vegetation species and site locations. Photochemical reduction of Hg^{2+} occurs in all terrestrial ecosystems,[16,34] as evidenced the scatter plot of Δ^{199}Hg versus Δ^{201}Hg that yields a slope of 1.0.[16,34,44] The foliage of different plant species shows similar isotopic signatures (Δ^{200}Hg = −0.02 ± 0.03‰ in tree foliage versus 0.01 ± 0.04‰ in others; Δ^{201}Hg = −0.24 ± 0.12‰ in tree foliage versus −0.20 ± 0.13‰ in others, SI Table S1, $p > 0.05$). The Hg MIF signatures in foliage at rural sites exhibit consistent values (SI Figure S1 and Figure 1) across the globe.

Intriguingly, samples of submerged vegetation and surface sediment from Tibetan wetlands exhibit positive Δ^{199}Hg and Δ^{200}Hg values (Figure 1), characteristic of the MIF signatures of Hg^{2+} in precipitation water, and indicating a possibility that atmospheric Hg^{2+} deposition is the dominant source. Estimates from the mixing model using Δ^{200}Hg (detailed in the SI) yields Hg^{2+} (through precipitation) and Hg^0 (through vegetative uptake) contributes 68 ± 21% and 32 ± 19% to vegetation Hg, respectively. The triple endmember mixing model using Δ^{199}Hg and Δ^{200}Hg (detailed in SI) suggests 26 ± 19% of surface soil Hg in Tibetan wetlands is from atmospheric Hg^0 deposition, 40 ± 17% from atmospheric Hg^{2+} deposition, and 34 ± 18% inherited from parent soil material. This is different from earlier studies which revealed that Hg in streams and runoffs from forest catchment is mainly derived from dry deposition of atmospheric Hg^0.[45,46] Mercury sources in Tibetan wetlands (mainly supplied by precipitation and glacier meltwater[47]) clearly distinct from those for forest surface soil, showing the characteristics of atmospheric Hg^{2+} deposition.

Surface soils in agricultural lands are mainly influenced by human activities, and therefore has elevated Hg concentrations (>200 ng g^{-1}) with isotopic signatures similar to Hg emission from anthropogenic sources (~0 Δ^{199}Hg and Δ^{201}Hg signatures, p = 0.324 by t test).[16,34,48] Except for Tibetan wetlands, the MIF signatures (Δ^{199}Hg and Δ^{200}Hg, Figure 1) of surface soil Hg in forest, peatland, grassland, and tundra ecosystems are more characteristic of vegetation rather than those found in atmospheric water (positive Δ^{199}Hg and Δ^{200}Hg)[14,16,34] and geological inputs (~0 Δ^{199}Hg and Δ^{200}Hg).[16,49] This suggests wet deposition of atmospheric Hg cannot explain the observed isotopic characteristics in soil samples. In addition, precipitation intensity is the dominant factor (rather than Hg concentration in precipitation) that leads to Hg wet deposition at remote sites globally.[6,7] If Hg input from precipitation contributed significantly to soil Hg, observed Δ^{199}Hg shift in surface soil samples would exhibit positive correlation to precipitation intensity. However, the data in this study show the opposite trend, as indicated by the negative correlation observed between precipitation and Δ^{199}Hg in rural forest and grassland ecosystems (r = −0.55, $p < 0.001$, n = 48 sites, SI Figure S3). Moreover, the triple endmember mixing model shows that 54 ± 21% (mean ±1 SD) of Hg in the surface soil of global documented ecosystems is derived from atmospheric Hg^0 deposition, 12 ± 9% from atmospheric Hg^{2+} deposition, and 34 ± 18% inherited from parent soil material. This is consistent with earlier findings that dry deposition of Hg^0 is the primary source of soil Hg.[14,19,21,22,36,37]

The significantly negative correlation between precipitation and Δ^{199}Hg can be explained by vegetative development enhanced by precipitation, which increases biomass production and therefore a greater atmospheric Hg^0 uptake vegetation that leads to more negative Δ^{199}Hg in surface soil after litterfall. Such evidence has been documented in earlier Hg isotope studies across North American forests and eastern Tibetan plateau forests that higher precipitation and warmer temperature enhance plant productivity and subsequently increase Hg accumulation in soil through atmospheric Hg^0 deposition through plant uptake.[8,9] Since the spatial distribution of vegetative development is closely tied to the climatic

DOI: 10.1021/acs.est.9b02386
Environ. Sci. Technol. 2019, 53, 10665−10675

factors,[25−28] the changed vegetation distribution will also be forced by climate change, thus shaping the soil surface Hg geospatial distribution.

3.2. Influences of Climate Change and Vegetation Development on soil Hg. It has been suggested that surface soil Hg concentration is correlated with soil organic carbon (SOC), leaf area index (LAI), plant net primary production (NPP), and anthropogenic Hg emission.[14,50−52] We categorized these factors into three groups: climate factors (e.g., precipitation, temperature, and solar irradiance), vegetation-related factors (e.g., LAI, NPP, and SOC), and human factors (e.g., population and anthropogenic Hg emission). Few studies have reported the interplays among surface soil Hg concentration and these factors at a continual or global scale. Cross analysis of data collected (n = 1541 1° × 1° grid cells) in China and the U.S. (SI Figure S2) shows that Hg concentration in surface soil is highly correlated to climate factors, moderately correlated to vegetation related factors, and weakly correlated to anthropogenic activities (population and anthropogenic Hg emission). This suggests that climate and vegetation play important roles in shaping the spatial distribution of Hg in surface soil.

Factors contributing to the spatial variation of soil Hg as explained by the structural equation modeling pathway network are shown in Figure 2. The direct effect by vegetation

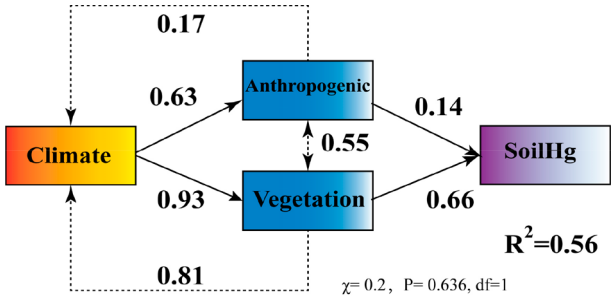

Figure 2. Structural equation modeling to explain the spatial distribution of surface soil Hg concentration. The solid arrow means the direct effect and the associated number is the standardized path coefficient (β), which represents the direct effect of one variable on another (highest as 1.0). The dotted arrow represents the feedback, and the number shows the strength of feedback effect (highest as 1.0). The double-headed arrow means the collineation between anthropogenic influence and vegetation, and the number shows the strength of collineation (highest as 1.0). All data have been logarithmically transformed to match the requirement of normal distribution in structural equation modeling model. Climate is the PCA component1 of mean annual precipitation, mean annual temperature, and solar radiation (SI Table S4). Anthropogenic influence is the PCA component 1 of mean annual emissions of Hg species and population (SI Table S5). Vegetation is the PCA component 1 of LAI, SOC, and NPP (SI Table S6).

is 0.66, compared to the much smaller effect by human activities (0.14). This suggests the direct impact from human activities is largely invisible over a large spatial scale. This is plausible, since anthropogenic emissions of Hg is primarily from point sources. In addition, the Hg isotopic data suggest wet deposition (removing GOM in the atmosphere generally) is less important than previously perceived as emissions are prone to long-range atmospheric transport. The variation of vegetation development is controlled by the climate factor (direct effect up to 0.93), leading to a confounded effect of climate-vegetation forcing at 0.61. This is much greater than the total effect of 0.09 by climate-human activities as indicated by the isotopic evidence that relates Hg accumulation in soil to vegetation productivity.

The high Hg^0 concentrations caused by anthropogenic Hg release in industrialized areas is greatly diluted during chemical transport processes over the long residence time of Hg^0 (0.5−1 year).[53] Dry deposition of Hg^0 via vegetation uptake is the main source for soil Hg accumulation in vegetated ecosystems. Since climate is a predominant driver for global vegetation distribution, the impact caused by the changing climate and subsequent vegetation distribution enriches soil Hg concentration in remote regions, such as Tibetan forests[14,54] and arctic tundra.[37,55] This is also supported by structural equation modeling results and Hg isotopic signatures at large scale.

Analytical results from the structural equation modeling also infer that climate has a strong impact on anthropogenic activities (direct effect = 0.63, Figure 2). The significant effect of climate on anthropogenic activities can be explained by population growth in the temperate climate zone. For example, regions with >800 mm precipitation in China make up only 43% of the land area, but have 94% of the population and substantially elevated soil Hg concentration.[11,56] Hence, this suggests some of the climate factors may actually be anthropogenic emissions hidden by climate changes. In addition, since human activities and vegetation development can impose feedback to climate in Figure 2, the climate-vegetation-human interactions are likely to occur under future land-use and climate change scenarios, which need to be considered when assessing global Hg cycling.

3.3. Climate and Vegetation Influence on Global Distribution of Hg in Surface soil. Using multivariate curvilinear regression and geospatial mapping (Section 2.2), global distribution of Hg concentration in top 0−20 cm surface soil is constructed using the WWF (World Wildlife Fund) 14 terrestrial ecoregion classifications. The Hg concentration in soil varies from 10 ng g^{-1} to 289 ng g^{-1} with a mean of 47 ± 26 ng g^{-1} and a median of 45 ng g^{-1} (Figure 3, SI Table S3). The model-predicted concentrations were verified using documented soil Hg spatial concentration data set in continental surface agricultural and grazing land soils in Europe, and at 740 sites values across the globe. Figure 3 shows that the histogram of simulated Hg concentration agrees with the observational data of continental surface soil in Europe. The scatterplot of model-predicted Hg concentration versus observation yields a slope of 0.71 (R^2 = 0.72, n = 740, p < 0.01), indicating that the simulation results appropriately capture the magnitude and spatial feature of observed Hg concentration in soil globally. It is noteworthy that crustal Hg content is not uniform globally, and the assumption of a mean value in the model is a limitation of the simulation. Further studies are needed to depict the crustal Hg distribution for further improving Hg pool estimates in global topsoil.

There are other uncertainties for the model-predicted Hg concentrations. One uncertainty stems from the sparse observational coverage and large variability across ecosystems and soil profiles. Another possible cause leading to the unexplained data variability is the coarse grid resolution (1° × 1°) incapable of producing the observed elevated concentration in cities, highly industrialized regions, and Hg mining areas. The highest estimated Hg concentration in a grid cell is 289 ng g^{-1}, up to 5 times smaller compared to the values measured in the polluted area.[57,58] Although such under-

DOI: 10.1021/acs.est.9b02386
Environ. Sci. Technol. 2019, 53, 10665−10675

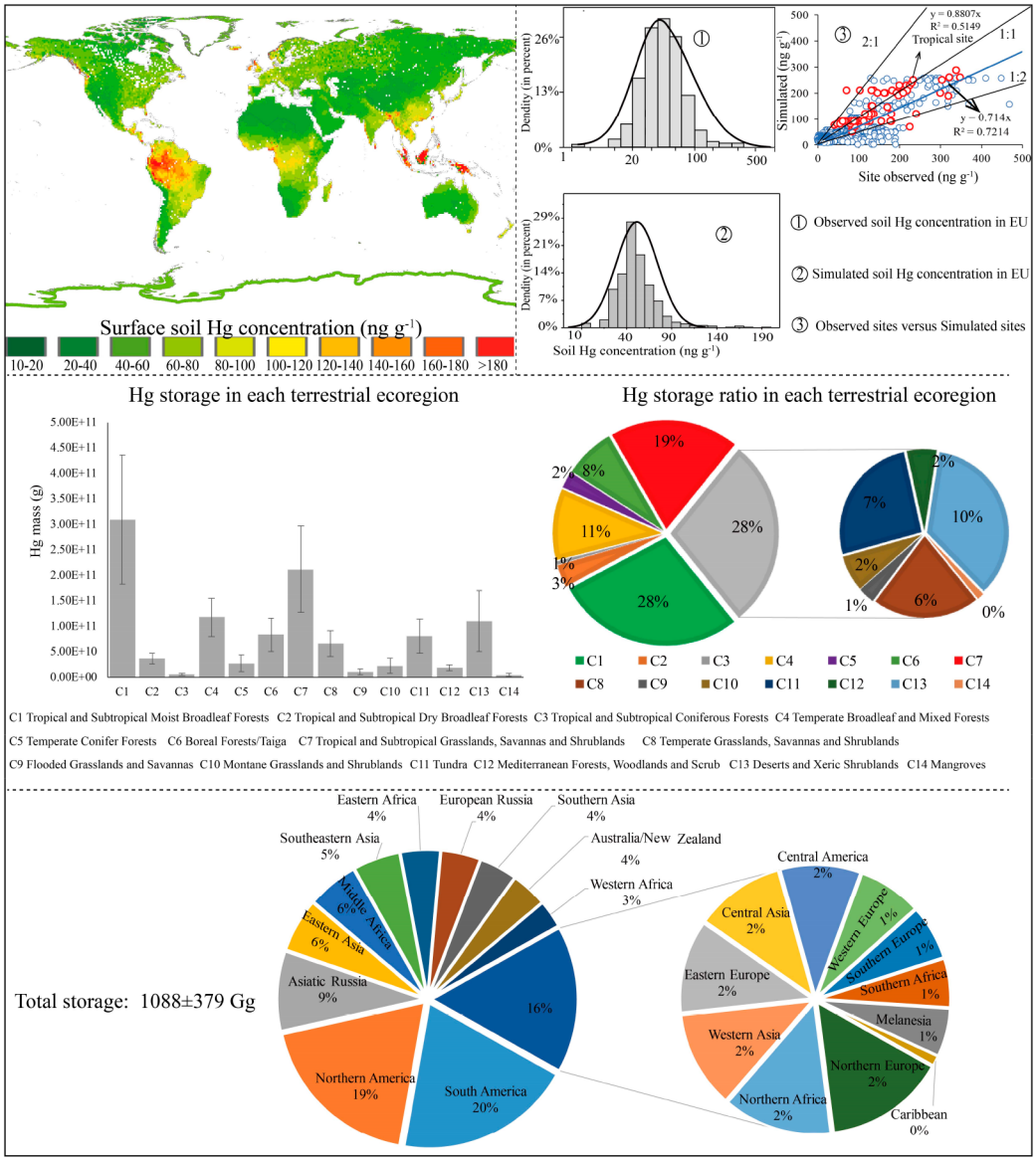

Figure 3. Simulated global 0−20 cm surface soil Hg concentration, WWF (World Wildlife Fund) 14 terrestrial ecoregions (SI Figure S4), and Hg storage in each terrestrial ecoregion and global region (SI Figure S5). The resolution of 0−20 cm surface soil Hg map is at the scale of 1° × 1°. The histogram of soil Hg concentration in agricultural and grazing soils of EU is reproduced from the earlier study.[88] The methods for collection of sites reported Hg concentrations were discussed in detail in the SI. The red circle in the plot of observations versus simulated values represents the data from tropical sites, and blue circle represents the data of from various forest sites across the globe.

estimation in selected regions does not significantly bias the estimated total storage size due to its small areal coverage (<1% of global surface),[59,60] it does contribute to the overall uncertainty of the estimate. Similarly, Hg concentration in soil measured in Hg mining area is 1−2 order of magnitude greater than the estimate in this study.[61,62] Finally, the limited observational data sets available in the tropical regions, tundra, and peatland introduce uncertainty to the present estimates. The statistical model was built using ∼52 000 points data, while only 2% of the data set was collected in tropical regions. However, the model-predicted soil Hg concentration in tropical forest regions falls in the range of 80−280 ng g^{-1}, consistent with the observed values (Figures 3, slope = 0.88, R^2 = 0.51, n = 74, p < 0.01).

The global pool of Hg stored in 0−20 cm surface soil is estimated to be 1088 ± 379 Gg. Thirty-two percent (32%) of estimated Hg storage in surface soil resides in tropical/subtropical forest regions (C1−C3 and C14, Figure 3), 23% in temperate/boreal forest regions (C4−C6 and C12), 28% in grassland and steppe and shrubland (C7−C10), 7% in tundra (C11), and 10% in desert and xeric shrubland (C13). Though relatively high soil Hg concentrations are observed in temperate forests (Figure 3), the low forest cover (9th largest) leads to Hg storage ranging in the medium level among 14 terrestrial ecoregions. Boreal ecoregion is fourth largest forest coverage, while the lower soil density results in fifth largest store of surface soil Hg.

The greater Hg storage in tropical/subtropical forest regions is consistent with the higher litterfall that drives a greater amount of Hg input to the forest soil. Global litterfall-induced Hg deposition is estimated at 1000−1200 Mg yr^{-1}, of which ∼70% occurs in tropical/subtropical forest ecosystems.[29,30] Observations mass balance assessments made in temperate and tropical regions showed that both types of forest act as a net

DOI: 10.1021/acs.est.9b02386
Environ. Sci. Technol. 2019, 53, 10665−10675

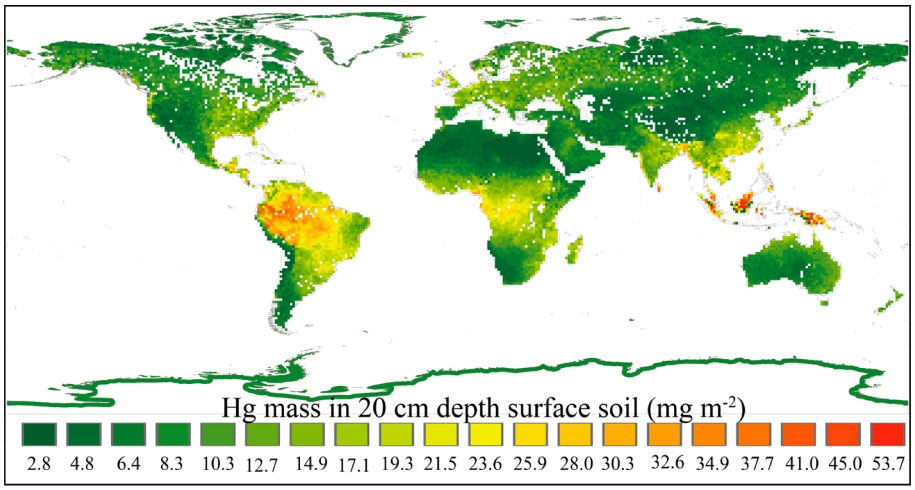

Figure 4. Simulated Hg mass in top 20 cm soils across the globe.

sink for atmospheric Hg, although the quantity of the sink differs.[4,20,63−66] The Hg input to surface soil from plant uptake and subsequent litterfall has been found to be several times higher than the Hg evasion flux.[66,67] In the tropical/subtropical forest, up to 70−95% of Hg deposition is stored in the forest floor,[20,63,64] and more than 75% of Hg depositions can be stored in forest floor of temperate/boreal regions.[65,68−70] These quantitative assessments point to the Hg input driven by vegetation activities being the main factor causing the observed Hg pool size, which also plausibly explain the greater Hg storage in tropical/subtropical forest regions.

As illustrated in Figure 3, half of Hg storage in surface soil is distributed in South America (20%), North America (19%), East Asia (6%), and Southeast Asia (5%). The larger land area covered by forest is the primary cause of the large Hg storage in South and North America. According to the 2013 Global Mercury Assessment (GMA 2013), anthropogenic Hg release in South, Southeast and East Asia accounts for ∼50% of global total in 2010, with China as the largest emitter.[71] Although elevated Hg concentrations in the soil of southern and eastern China (100−200 ng g^{-1}) exist, the mean Hg concentration in mainland China (44 ± 28 ng g^{-1}) is comparable to the value (all $p > 0.05$) in the U.S. (43 ± 24 ng g^{-1}) and Europe (47 ± 23 ng g^{-1}). There are two possible explanations. One is that the sum of anthropogenic Hg release in U.S. and Europe after industrial revolution is 2−3 times higher than total emissions in China.[72] The other is that the dense vegetation biomass in the U.S. and Europe induce a greater amount of Hg accumulation in soil through atmospheric Hg^0 uptake by foliage. Forest coverage in the U.S. and Europe (34−40%) is substantially higher than the coverage in China (22%).[73] A larger area of permafrost soil in U.S. and Europe, where elevated Hg is locked in soil over thousands of years of accumulation of dead plant and animal matter,[12] also contributed to the Hg storage in soil.

3.4. Comparison with Previous Model Results. An earlier study estimated up to 347 ± 146 Gg Hg storage in top 30 cm permafrost soil in the northern hemisphere,[12] much higher than our estimate in top 20 cm soils of Tundra (80.1 ± 33.5 Gg). Such a difference is mainly caused by different classification of the terrestrial ecoregion (24.8 million km^2[12] versus 11.7 million km^2 in this study) and the soil depth (30 cm[12] versus 20 cm in this study). Our predicted Hg storage in top 20 cm soils in Arctic tundra is 48.8 ± 21.5 Gg in Figure 3, consistent with the estimate based on filed observation (25.8−41.9 Gg for 50th-62.5th).[55]

Earlier estimates of Hg stored in global surface soil ranges from 235 to 1150 Gg.[3,5−8] These estimates have inherited uncertainties due to sparse observational coverage and variabilities across ecosystems and soil profiles. For example, the Hg/C ratio is widely used for such estimates,[3,6,7] but it changes considerably with soil depth and land-use type.[20,50,74] Also, Hg/C ratio data are not sufficiently documented for grassland, shrubland, desert, cropland, etc. The global soil Hg spatial distribution produced by Global Terrestrial Mercury Model (GTMM) used in GEOS-Chem predicted a low Hg storage (0−2 mg m^{-2}) in top 30 cm soil of temperate/boreal regions (45−70 $N°$) and large storage (2−14 mg m^{-2}) in arid areas of north Africa, western Asia, and southern Asia.[6] Figure 4 shows that the simulated Hg storage in top 20 cm soil in temperate/boreal regions is 4−15 mg m^{-2}, and 0−3 mg m^{-2} in arid areas of northern Africa, western Asia, and southern Asia. Our estimates agree with the geological survey results that show Hg concentration in soil of arid regions is significantly lower than those observed in vegetation areas.[11,50] The large data sets of climate and geospatial features applied in this study improve the accuracy of our estimate.

4. IMPLICATIONS

Present and future human activities will likely irreversibly change the climate and global vegetation coverage. The confounded impacts among the climate-vegetation-human activities (Figure 2) may significantly alter global Hg cycling. For example, the terrestrial net carbon sink accelerated during 1998−2012 (0.17 ± 0.05 Pg C yr^{-2}) due to the decreased tropical forest area, CO_2 fertilization, and increased afforestation in the northern temperate regions.[25,26,75] Given an average of ∼50 ng g^{-1} C of Hg/C ratio,[23,66] we estimate ∼8.5 Mg $yr^{-1}$of Hg sink in global terrestial ecosystems during this period. The potential impact of increasing temperature on the magnitude and direction of air−soil Hg^0 flux is not clearly understood.[76] Eariler studies have highlighted soil Hg re-emission and Hg runoff both increased 2−5 times due to landuse changes[77−79] at local sites, while global assessment of these terms are largely lacking.

Anthropogenic Hg release into the atmosphere is relatively well understood.[72,80] Results from regional and global Hg

DOI: 10.1021/acs.est.9b02386
Environ. Sci. Technol. 2019, 53, 10665−10675

modeling studies have also depicted the patterns of anthropogenic Hg emission transport and deposition.[81−83] In contrast, natural Hg processes in terrestrial ecosystems have not been well constrained, leading to substantial uncertainties in global Hg biogeochemical cycling. This study constructs Hg storage in global surface soil and its spatial distribution driven by climate and vegetation, and provides conceptual parametrization to develop a more comprehensive global Hg modeling system that can systematically incorporate climate-vegetation-human impacts. Earlier studies have shown an increase in Hg fluxes during the transition from the Holocene to the Anthropocene.[31−33] This study has important implications on the response of Hg to future emissions declines and climate-vegetation changes. Anthropogenic Hg emission is projected to decrease aggressively through the implementation of *Minamata Convention*, but the decrease in Hg storage and its exposure to human and wildlife will take a much longer period due to the legacy Hg cycling in the global environment, especially under the scenarios of changing climate.

■ ASSOCIATED CONTENT

Supporting Information

. The Supporting Information is available free of charge on the ACS Publications website at DOI: 10.1021/acs.est.9b02386.

Measurement, Hg MIF mixing models, data collection, and availability; Tables S1−S7 and Figures S1−S5 (PDF)

■ AUTHOR INFORMATION

Corresponding Author

*E-mail: fengxinbin@vip.skleg.cn.

ORCID

Xun Wang: 0000-0002-7407-8965

Leiming Zhang: 0000-0001-5437-5412

Xinbin Feng: 0000-0002-7462-8998

Notes

The authors declare no competing financial interest.

■ ACKNOWLEDGMENTS

This work was funded by the Strategic Priority Research Programs of Chinese Academy of Sciences, Pan-Third Pole Environment Study for a Green Silk Road (Pan-TPE, XDA2004050201),National Natural Science Foundation of China (41829701, 41703135, and 41771062), K.C.Wong Education Foundation, and China Postdoctoral Science Foundation (BX201700235 and 2017M620432).We thank the sampling help from Mt. Ailao Station, Mt. Gongga Station, Linzhi Station, Shenzha Station, Cele Station, Yanchi Station, Xilingele Station, Changshu Station, Yingtan Station, Chengkou Station in National Ecosystem Research Network of China and in Chinese Desert & Grassland Ecosystem Research Station Alliance. We thank Dr. Zhengde Jiang from Institute of Applied Ecology, Chinese Academy of Sciences, and Dr. Jun Zhou and Dr. Shuwei Wang from Institute of Soil Science, Chinese Academy of Sciences for assistance during sampling.

■ REFERENCES

(1) Selin, H.; Keane, S. E.; Wang, S. X.; Selin, N. E.; Davis, K.; Bally, D. Linking science and policy to support the implementation of the Minamata Convention on Mercury. *Ambio* **2018**, *47* (2), 198−215.

(2) Selin, N. E. A proposed global metric to aid mercury pollution policy. *Science* **2018**, *360* (6389), 607−609.

(3) Amos, H. M.; Sonke, J. E.; Obrist, D.; Robins, N.; Hagan, N.; Horowitz, H. M.; Mason, R. P.; Witt, M.; Hedgecock, I. M.; Corbitt, E. S.; Sunderland, E. M. Observational and Modeling Constraints on Global Anthropogenic Enrichment of Mercury. *Environ. Sci. Technol.* **2015**, *49* (7), 4036−4047.

(4) Obrist, D.; Kirk, J. L.; Zhang, L.; Sunderland, E. M.; Jiskra, M.; Selin, N. E. A review of global environmental mercury processes in response to human and natural perturbations: Changes of emissions, climate, and land use. *Ambio* **2018**, *47* (2), 116−140.

(5) Amos, H. M.; Jacob, D. J.; Streets, D. G.; Sunderland, E. M. Legacy impacts of all-time anthropogenic emissions on the global mercury cycle. *Global Biogeochem Cy* **2013**, *27* (2), 410−421.

(6) Smith-Downey, N. V.; Sunderl, E. M.; Jacob, D. J. Anthropogenic impacts on global storage and emissions of mercury from terrestrial soils: Insights from a new global model. *J. Geophys. Res.* **2010**, *115* (G3), 227−235.

(7) Hararuk, O.; Obrist, D.; Luo, Y. Modelling the sensitivity of soil mercury storage to climate-induced changes in soil carbon pools. *Biogeosciences* **2013**, *10* (4), 2393−2407.

(8) Selin, N. E.; Jacob, D. J.; Yantosca, R. M.; Strode, S.; Jaegle, L.; Sunderland, E. M., Global 3-D land-ocean-atmosphere model for mercury: Present-day versus preindustrial cycles and anthropogenic enrichment factors for deposition. *Global Biogeochem. Cycles* **2008**, *22*, (2),

(9) Lindberg, S.; Bullock, R.; Ebinghaus, R.; Engstrom, D.; Feng, X. B.; Fitzgerald, W.; Pirrone, N.; Prestbo, E.; Seigneur, C. A synthesis of progress and uncertainties in attributing the sources of mercury in deposition. *Ambio* **2007**, *36* (1), 19−32.

(10) Li, P.; Du, B. Y.; Chan, H. M.; Feng, X. B. Human inorganic mercury exposure, renal effects and possible pathways in Wanshan mercury mining area, China. *Environ. Res.* **2015**, *140*, 198−204.

(11) Wang, X. Q.; Liu, X. M.; Han, Z. X.; Zhou, J.; Xu, S. F.; Zhang, Q.; Chen, H. J.; Bo, W.; Xia, X. Concentration and distribution of mercury in drainage catchment sediment and alluvial soil of China. *J. Geochem. Explor.* **2015**, *154*, 32−48.

(12) Schuster, P. F.; Schaefer, K. M.; Aiken, G. R.; Antweiler, R. C.; Dewild, J. F.; Gryziec, J. D.; Gusmeroli, A.; Hugelius, G.; Jafarov, E.; Krabbenhoft, D. P.; Liu, L.; Herman-Mercer, N.; Mu, C.; Roth, D. A.; Schaefer, T.; Striegl, R. G.; Wickland, K. P.; Zhang, T. Permafrost Stores a Globally Significant Amount of Mercury. *Geophys. Res. Lett.* **2018**, *45* (3), 1463−1471.

(13) Smith, D. B.; Cannon, W. F.; Woodruff, L. G.; Solano, F.; Ellefsen, K. J. *Geochemical and Mineralogical Maps for Soils of the Conterminous United States*; 2014−1082; Reston, VA, 2014; p 399.

(14) Wang, X.; Luo, J.; Yin, R.; Yuan, W.; Lin, C.-J.; Sommar, J.; Feng, X.; Wang, H.; Lin, C. Using Mercury Isotopes To Understand Mercury Accumulation in the Montane Forest Floor of the Eastern Tibetan Plateau. *Environ. Sci. Technol.* **2017**, *51* (2), 801−809.

(15) Zhang, L. M.; Wu, Z. Y.; Cheng, I.; Wright, L. P.; Olson, M. L.; Gay, D. A.; Risch, M. R.; Brooks, S.; Castro, M. S.; Conley, G. D.; Edgerton, E. S.; Holsen, T. M.; Luke, W.; Tordon, R.; Weiss-Penzias, P. The Estimated Six-Year Mercury Dry Deposition Across North America. *Environ. Sci. Technol.* **2016**, *50* (23), 12864−12873.

(16) Blum, J. D.; Sherman, L. S.; Johnson, M. W. Mercury Isotopes in Earth and Environmental Sciences. *Annu. Rev. Earth Planet. Sci.* **2014**, *42*, 249−269.

(17) Lu, X. K.; Yang, M.; Shi, J. A.; Feng, X. O. The Effect of Huanghe River Runoff on the Occurrence, Transportation and Speciation of Mercury in the Huanghe Estuary and Adjacent Sea. *Geochem. J.* **1990**, *24* (4), 295−308.

(18) Sprovieri, F.; Pirrone, N.; Bencardino, M.; D'Amore, F.; Angot, H.; Barbante, C.; Brunke, E. G.; Arcega-Cabrera, F.; Cairns, W.; Comero, S.; Dieguez, M. D.; Dommergue, A.; Ebinghaus, R.; Feng, X. B.; Fu, X. W.; Garcia, P. E.; Gawlik, B. M.; Hagestrom, U.; Hansson, K.; Horvat, M.; Kotnik, J.; Labuschagne, C.; Magand, O.; Martin, L.; Mashyanov, N.; Mkololo, T.; Munthe, J.; Obolkin, V.; Islas, M. R.; Sena, F.; Somerset, V.; Spandow, P.; Varde, M.; Walters, C.;

DOI: 10.1021/acs.est.9b02386
Environ. Sci. Technol. 2019, 53, 10665−10675

Wangberg, I.; Weigelt, A.; Yang, X.; Zhang, H. Five-year records of mercury wet deposition flux at GMOS sites in the Northern and Southern hemispheres. *Atmos. Chem. Phys.* **2017**, *17* (4), 2689−2708.
(19) Jiskra, M.; Wiederhold, J. G.; Skyllberg, U.; Kronberg, R.-M.; Hajdas, I.; Kretzschmar, R. Mercury Deposition and Re-emission Pathways in Boreal Forest Soils Investigated with Hg Isotope Signatures. *Environ. Sci. Technol.* **2015**, *49* (12), 7188−7196.
(20) Wang, X.; Lin, C.-J.; Lu, Z.; Zhang, H.; Zhang, Y.; Feng, X. Enhanced accumulation and storage of mercury on subtropical evergreen forest floor: Implications on mercury budget in global forest ecosystems. *J. Geophys. Res.: Biogeosci.* **2016**, *121* (8), 2096−2109.
(21) Zheng, W.; Obrist, D.; Weis, D.; Bergquist, B. A. Mercury isotope compositions across North American forests. *Global Biogeochem Cy* **2016**, *30* (10), 1475−1492.
(22) Zhang, H.; Yin, R. S.; Feng, X. B.; Sommar, J.; Anderson, C. W. N.; Sapkota, A.; Fu, X. W.; Larssen, T. Atmospheric mercury inputs in montane soils increase with elevation: evidence from mercury isotope signatures. *Sci. Rep.* **2013**, *3*, 3322.
(23) Jiskra, M.; Sonke, J. E.; Obrist, D.; Bieser, J.; Ebinghaus, R.; Myhre, C. L.; Pfaffhuber, K. A.; Wangberg, I.; Kyllonen, K.; Worthy, D.; Martin, L. G.; Labuschagne, C.; Mkololo, T.; Ramonet, M.; Magand, O.; Dommergue, A. A vegetation control on seasonal variations in global atmospheric mercury concentrations. *Nat. Geosci.* **2018**, *11* (4), 244−250.
(24) Obrist, D. Atmospheric mercury pollution due to losses of terrestrial carbon pools? *Biogeochemistry* **2007**, *85* (2), 119−123.
(25) Ding, J. Z.; Chen, L. Y.; Ji, C. J.; Hugelius, G.; Li, Y. N.; Liu, L.; Qin, S. Q.; Zhang, B. B.; Yang, G. B.; Li, F.; Fang, K.; Chen, Y. L.; Peng, Y. F.; Zhao, X.; He, H. L.; Smith, P.; Fang, J. Y.; Yang, Y. H. Decadal soil carbon accumulation across Tibetan permafrost regions. *Nat. Geosci.* **2017**, *10* (6), 420−424.
(26) Piao, S.; Huang, M.; Liu, Z.; Wang, X.; Ciais, P.; Canadell, J. G.; Wang, K.; Bastos, A.; Friedlingstein, P.; Houghton, R. A.; Le Quéré, C.; Liu, Y.; Myneni, R. B.; Peng, S.; Pongratz, J.; Sitch, S.; Yan, T.; Wang, Y.; Zhu, Z.; Wu, D.; Wang, T. Lower land-use emissions responsible for increased net land carbon sink during the slow warming period. *Nat. Geosci.* **2018**, *11* (10), 739−743.
(27) Gottfried, M.; Pauli, H.; Futschik, A.; Akhalkatsi, M.; Barančok, P.; Benito Alonso, J. L.; Coldea, G.; Dick, J.; Erschbamer, B.; Fernández Calzado, M. a. R.; Kazakis, G.; Krajči, J.; Larsson, P.; Mallaun, M.; Michelsen, O.; Moiseev, D.; Moiseev, P.; Molau, U.; Merzouki, A.; Nagy, L.; Nakhutsrishvili, G.; Pedersen, B.; Pelino, G.; Puscas, M.; Rossi, G.; Stanisci, A.; Theurillat, J.-P.; Tomaselli, M.; Villar, L.; Vittoz, P.; Vogiatzakis, I.; Grabherr, G. Continent-wide response of mountain vegetation to climate change. *Nat. Clim. Change* **2012**, *2*, 111−115.
(28) Theurillat, J.-P.; Guisan, A. Potential Impact of Climate Change on Vegetation in the European Alps: A Review. *Clim. Change* **2001**, *50* (1), 77−109.
(29) Wang, X.; Bao, Z. D.; Lin, C. J.; Yuan, W.; Feng, X. B. Assessment of Global Mercury Deposition through Litterfall. *Environ. Sci. Technol.* **2016**, *50* (16), 8548−8557.
(30) Fu, X.; Zhu, W.; Zhang, H.; Sommar, J.; Yu, B.; Yang, X.; Wang, X.; Lin, C.-J.; Feng, X. Depletion of atmospheric gaseous elemental mercury by plant uptake at Mt. Changbai, Northeast China. *Atmos. Chem. Phys.* **2016**, *16* (20), 12861−12873.
(31) Rydberg, J.; Rosch, M.; Heinz, E.; Biester, H. Influence of catchment vegetation on mercury accumulation in lake sediments from a long-term perspective. *Sci. Total Environ.* **2015**, *538*, 896−904.
(32) Cooke, C. A.; Balcom, P. H.; Biester, H.; Wolfe, A. P. Over three millennia of mercury pollution in the Peruvian Andes. *Proc. Natl. Acad. Sci. U. S. A.* **2009**, *106* (22), 8830−8834.
(33) Pompeani, D. P.; Cooke, C. A.; Abbott, M. B.; Drevnick, P. E. Climate, Fire, and Vegetation Mediate Mercury Delivery to Midlatitude Lakes over the Holocene. *Environ. Sci. Technol.* **2018**, *52* (15), 8157−8164.
(34) Sonke, J. E. A global model of mass independent mercury stable isotope fractionation. *Geochim. Cosmochim. Acta* **2011**, *75* (16), 4577−4590.
(35) Yang, Y.; Yanai, R. D.; Montesdeoca, M.; Driscoll, C. T. Measuring mercury in wood: challenging but important. *Int. J. Environ. Anal. Chem.* **2017**, *97* (5), 456−467.
(36) Enrico, M.; Le Roux, G.; Marusczak, N.; Heimburger, L. E.; Claustres, A.; Fu, X. W.; Sun, R. Y.; Sonke, J. E. Atmospheric Mercury Transfer to Peat Bogs Dominated by Gaseous Elemental Mercury Dry Deposition. *Environ. Sci. Technol.* **2016**, *50* (5), 2405−2412.
(37) Obrist, D.; Agnan, Y.; Jiskra, M.; Olson, C. L.; Colegrove, D. P.; Hueber, J.; Moore, C. W.; Sonke, J. E.; Helmig, D. Tundra uptake of atmospheric elemental mercury drives Arctic mercury pollution. *Nature* **2017**, *547* (7662), 201−204.
(38) Guédron, S.; Amouroux, D.; Tessier, E.; Grimaldi, C.; Barre, J.; Berail, S.; Perrot, V.; Grimaldi, M. Mercury Isotopic Fractionation during Pedogenesis in a Tropical Forest Soil Catena (French Guiana): Deciphering the Impact of Historical Gold Mining. *Environ. Sci. Technol.* **2018**, *52* (20), 11573−11582.
(39) Demers, J. D.; Blum, J. D.; Zak, D. R. Mercury isotopes in a forested ecosystem: Implications for air-surface exchange dynamics and the global mercury cycle. *Global Biogeochem Cy* **2013**, *27* (1), 222−238.
(40) Blum, J. D.; Bergquist, B. A. Reporting of variations in the natural isotopic composition of mercury. *Anal. Bioanal. Chem.* **2007**, *388* (2), 353−359.
(41) Estrade, N.; Carignan, J.; Sonke, J. E.; Donard, O. F. X. Measuring Hg Isotopes in Bio-Geo-Environmental Reference Materials. *Geostand. Geoanal. Res.* **2010**, *34* (1), 79−93.
(42) UNEP *Global Mercury Assessment 2013: Sources, Emissions, Releases and Environmental Transport*; UNEP Chemicals Branch: Geneva, Switzerland, 2013; p 44.
(43) Reimann, C.; de Caritat, P. Establishing geochemical background variation and threshold values for 59 elements in Australian surface soil. *Sci. Total Environ.* **2017**, *578*, 633−648.
(44) Sun, R.; Jiskra, M.; Amos, H. M.; Zhang, Y.; Sunderland, E. M.; Sonke, J. E. Modelling the mercury stable isotope distribution of Earth surface reservoirs: Implications for global Hg cycling. *Geochim. Cosmochim. Acta* **2019**, *246*, 156−173.
(45) Woerndle, G. E.; Tsz-Ki Tsui, M.; Sebestyen, S. D.; Blum, J. D.; Nie, X.; Kolka, R. K. New Insights on Ecosystem Mercury Cycling Revealed by Stable Isotopes of Mercury in Water Flowing from a Headwater Peatland Catchment. *Environ. Sci. Technol.* **2018**, *52* (4), 1854−1861.
(46) Jiskra, M.; Wiederhold, J. G.; Skyllberg, U.; Kronberg, R.-M.; Kretzschmar, R. Source tracing of natural organic matter bound mercury in boreal forest runoff with mercury stable isotopes. *Environmental Science: Processes & Impacts* **2017**, *19* (10), 1235−1248.
(47) Zhang, Q. G.; Huang, J.; Wang, F. Y.; Mark, L. W.; Xu, J. Z.; Armstrong, D.; Li, C. L.; Zhang, Y. L.; Kang, S. C. Mercury Distribution and Deposition in Glacier Snow over Western China. *Environ. Sci. Technol.* **2012**, *46* (10), 5404−5413.
(48) Yu, B.; Fu, X.; Yin, R.; Zhang, H.; Wang, X.; Lin, C.-J.; Wu, C.; Zhang, Y.; He, N.; Fu, P. Isotopic composition of atmospheric mercury in China: new evidence for sources and transformation processes in air and in vegetation. *Environ. Sci. Technol.* **2016**, *50* (17), 9262−9269.
(49) Smith, C. N.; Kesler, S. E.; Blum, J. D.; Rytuba, J. J. Isotope geochemistry of mercury in source rocks, mineral deposits and spring deposits of the California Coast Ranges, USA. *Earth Planet. Sci. Lett.* **2008**, *269* (3−4), 398−406.
(50) Obrist, D.; Pearson, C.; Webster, J.; Kane, T.; Lin, C. J.; Aiken, G. R.; Alpers, C. N. A synthesis of terrestrial mercury in the western United States: Spatial distribution defined by land cover and plant productivity. *Sci. Total Environ.* **2016**, *568*, 522−535.
(51) Navrátil, T.; Shanley, J.; Rohovec, J.; Hojdová, M.; Penížek, V.; Buchtová, J. Distribution and Pools of Mercury in Czech Forest Soils. *Water, Air, Soil Pollut.* **2014**, *225* (3), 1829.
(52) Yu, X.; Driscoll, C. T.; Warby, R. A. F.; Montesdeoca, M.; Johnson, C. E. Soil mercury and its response to atmospheric mercury deposition across the northeastern United States. *Ecol Appl.* **2014**, *24* (4), 812−822.

DOI: 10.1021/acs.est.9b02386
Environ. Sci. Technol. 2019, 53, 10665−10675

(53) Sprovieri, F.; Pirrone, N.; Bencardino, M.; D'Amore, F.; Carbone, F.; Cinnirella, S.; Mannarino, V.; Landis, M.; Ebinghaus, R.; Weigelt, A.; Brunke, E. G.; Labuschagne, C.; Martin, L.; Munthe, J.; Wängberg, I.; Artaxo, P.; Morais, F.; Barbosa, H. D. M. J.; Brito, J.; Cairns, W.; Barbante, C.; Diéguez, M. D. C.; Garcia, P. E.; Dommergue, A.; Angot, H.; Magand, O.; Skov, H.; Horvat, M.; Kotnik, J.; Read, K. A.; Neves, L. M.; Gawlik, B. M.; Sena, F.; Mashyanov, N.; Obolkin, V.; Wip, D.; Feng, X. B.; Zhang, H.; Fu, X.; Ramachandran, R.; Cossa, D.; Knoery, J.; Marusczak, N.; Nerentorp, M.; Norstrom, C. Atmospheric mercury concentrations observed at ground-based monitoring sites globally distributed in the framework of the GMOS network. *Atmos. Chem. Phys.* **2016**, *16* (18), 11915−11935.
(54) Gong, P.; Wang, X. P.; Xue, Y. G.; Xu, B. Q.; Yao, T. D. Mercury distribution in the foliage and soil profiles of the Tibetan forest: Processes and implications for regional cycling. *Environ. Pollut.* **2014**, *188*, 94−101.
(55) Olson, C.; Jiskra, M.; Biester, H.; Chow, J.; Obrist, D. Mercury in Active-Layer Tundra Soils of Alaska: Concentrations, Pools, Origins, and Spatial Distribution. *Global Biogeochem Cy* **2018**, *32* (7), 1058−1073.
(56) Wang; Guixin; Zehem. The Robustness of China's Migration and Heihe-Tengchong Line. *China Population Today* **2016**, *4*, 39−39.
(57) Feng, X. B.; Tang, S. L.; Li, Z. G.; Wang, S. F.; Liang, L. Landfill is an important atmospheric mercury emission source. *Chin. Sci. Bull.* **2004**, *49* (19), 2068−2072.
(58) Wang, J. X.; Feng, X. B.; Anderson, C. W. N.; Xing, Y.; Shang, L. H. Remediation of mercury contaminated sites - A review. *J. Hazard. Mater.* **2012**, *221*, 1−18.
(59) Liu, Z.; He, C.; Zhou, Y.; Wu, J. How much of the world's land has been urbanized, really? A hierarchical framework for avoiding confusion. *Landscape Ecology* **2014**, *29* (5), 763−771.
(60) Schneider, A.; Friedl, M. A.; Potere, D. A new map of global urban extent from MODIS satellite data. *Environ. Res. Lett.* **2009**, *4* (4), 44003−44010.
(61) Dai, Z. H.; Feng, X. B.; Sommar, J.; Li, P.; Fu, X. W. Spatial distribution of mercury deposition fluxes in Wanshan Hg mining area, Guizhou province, China. *Atmos. Chem. Phys.* **2012**, *12* (14), 6207−6218.
(62) Feng, X. B.; Qiu, G. L. Mercury pollution in Guizhou, Southwestern China - An overview. *Sci. Total Environ.* **2008**, *400* (1−3), 227−237.
(63) Ma, M.; Wang, D. Y.; Du, H. X.; Sun, T.; Zhao, Z.; Wang, Y. M.; Wei, S. Q. Mercury dynamics and mass balance in a subtropical forest, southwestern China. *Atmos. Chem. Phys.* **2016**, *16* (7), 4529−4537.
(64) Silva, G. S. d.; Bisinoti, M. C.; Fadini, P. S.; Magarelli, G.; Jardim, W. F.; Fostier, A. H. Major aspects of the mercury cycle in the Negro River Basin, Amazon. *J. Braz. Chem. Soc.* **2009**, *20*, 1127−1134.
(65) Grigal, D. F. Mercury sequestration in forests and peatlands: A review. *J. Environ. Qual.* **2003**, *32* (2), 393−405.
(66) Wang, X.; Yuan, W.; Feng, X. Global Review of Mercury Biogeochemical Processes in Forest Ecosystems. *Prog. Chem.* **2017**, *29* (9), 970−980.
(67) Agnan, Y.; Le Dantec, T.; Moore, C. W.; Edwards, G. C.; Obrist, D. New Constraints on Terrestrial Surface Atmosphere Fluxes of Gaseous Elemental Mercury Using a Global Database. *Environ. Sci. Technol.* **2016**, *50* (2), 507−524.
(68) Schwesig, D.; Matzner, E. Pools and fluxes of mercury and methylmercury in two forested catchments in Germany. *Sci. Total Environ.* **2000**, *260* (1−3), 213−223.
(69) St Louis, V. L.; Rudd, J. W. M.; Kelly, C. A.; Hall, B. D.; Rolfhus, K. R.; Scott, K. J.; Lindberg, S. E.; Dong, W. Importance of the forest canopy to fluxes of methyl mercury and total mercury to boreal ecosystems. *Environ. Sci. Technol.* **2001**, *35* (15), 3089−3098.
(70) Fain, X.; Obrist, D.; Pierce, A.; Barth, C.; Gustin, M. S.; Boyle, D. P. Whole-watershed mercury balance at Sagehen Creek, Sierra Nevada, CA. *Geochim. Cosmochim. Acta* **2011**, *75* (9), 2379−2392.
(71) De Simone, F.; Gencarelli, C. N.; Hedgecock, I. M.; Pirrone, N. A Modeling Comparison of Mercury Deposition from Current Anthropogenic Mercury Emission Inventories. *Environ. Sci. Technol.* **2016**, *50* (10), 5154−5162.
(72) Streets, D. G.; Devane, M. K.; Lu, Z. F.; Bond, T. C.; Sunderland, E. M.; Jacob, D. J. All-Time Releases of Mercury to the Atmosphere from Human Activities. *Environ. Sci. Technol.* **2011**, *45* (24), 10485−10491.
(73) Keenan, R. J.; Reams, G. A.; Achard, F.; de Freitas, J. V.; Grainger, A.; Lindquist, E. Dynamics of global forest area: Results from the FAO Global Forest Resources Assessment 2015. *For. Ecol. Manage.* **2015**, *352*, 9−20.
(74) Obrist, D.; Johnson, D. W.; Lindberg, S. E.; Luo, Y.; Hararuk, O.; Bracho, R.; Battles, J. J.; Dail, D. B.; Edmonds, R. L.; Monson, R. K.; Ollinger, S. V.; Pallardy, S. G.; Pregitzer, K. S.; Todd, D. E. Mercury Distribution Across 14 US Forests. Part I: Spatial Patterns of Concentrations in Biomass, Litter, and Soils. *Environ. Sci. Technol.* **2011**, *45* (9), 3974−3981.
(75) Zhao, M. S.; Running, S. W. Drought-Induced Reduction in Global Terrestrial Net Primary Production from 2000 Through 2009. *Science* **2010**, *329* (5994), 940−943.
(76) Haynes, K. M.; Kane, E. S.; Potvin, L.; Lilleskov, E. A.; Kolka, R. K.; Mitchell, C. P. J. Gaseous mercury fluxes in peatlands and the potential influence of climate change. *Atmos. Environ.* **2017**, *154*, 247−259.
(77) Kronberg, R.-M.; Drott, A.; Jiskra, M.; Wiederhold, J. G.; Bjorn, E.; Skyllberg, U. Forest harvest contribution to Boreal freshwater methyl mercury load. *Global Biogeochem Cy* **2016**, *30* (6), 825−843.
(78) Mazur, M.; Mitchell, C. P. J.; Eckley, C. S.; Eggert, S. L.; Kolka, R. K.; Sebestyen, S. D.; Swain, E. B. Gaseous mercury fluxes from forest soils in response to forest harvesting intensity: A field manipulation experiment. *Sci. Total Environ.* **2014**, *496*, 678−687.
(79) Carpi, A.; Fostier, A. H.; Orta, O. R.; dos Santos, J. C.; Gittings, M. Gaseous mercury emissions from soil following forest loss and land use changes: Field experiments in the United States and Brazil. *Atmos. Environ.* **2014**, *96*, 423−429.
(80) Streets, D. G.; Zhang, Q.; Wu, Y. Projections of Global Mercury Emissions in 2050. *Environ. Sci. Technol.* **2009**, *43* (8), 2983−2988.
(81) Selin, N. E.; Sunderland, E. M.; Knightes, C. D.; Mason, R. A. Sources of Mercury Exposure for US Seafood Consumers: Implications for Policy. *Environ. Health Perspect.* **2010**, *118* (1), 137−143.
(82) Strode, S.; Jaegle, L.; Selin, N. E. Impact of mercury emissions from historic gold and silver mining: Global modeling. *Atmos. Environ.* **2009**, *43* (12), 2012−2017.
(83) Wang, X.; Lin, C.-J.; Feng, X.; Yuan, W.; Fu, X.; Zhang, H.; Wu, Q.; Wang, S. Assessment of Regional Mercury Deposition and Emission Outflow in Mainland China. *Journal of Geophysical Research: Atmospheres* **2018**, *123* (17), 9868−9890.
(84) Chen, J. B.; Hintelmann, H.; Feng, X. B.; Dimock, B. Unusual fractionation of both odd and even mercury isotopes in precipitation from Peterborough, ON, Canada. *Geochim. Cosmochim. Acta* **2012**, *90*, 33−46.
(85) Yuan, S. L.; Zhang, Y.; Chen, J. B.; Kang, S. C.; Zhang, J.; Feng, X.; Cai, H.; Wang, Z.; Wang, Z.; Huang, Q. Large Variation of Mercury Isotope Composition During a Single Precipitation Event at Lhasa City, Tibetan Plateau, China. *Procedia Earth Planet. Sci.* **2015**, *13*, 282−286.
(86) Gratz, L. E.; Keeler, G. J.; Blum, J. D.; Sherman, L. S. Isotopic Composition and Fractionation of Mercury in Great Lakes Precipitation and Ambient Air. *Environ. Sci. Technol.* **2010**, *44* (20), 7764−7770.
(87) Sherman, L. S.; Blum, J. D.; Keeler, G. J.; Demers, J. D.; Dvonch, J. T. Investigation of Local Mercury Deposition from a Coal-Fired Power Plant Using Mercury Isotopes. *Environ. Sci. Technol.* **2012**, *46* (1), 382−390.

DOI: 10.1021/acs.est.9b02386
Environ. Sci. Technol. 2019, 53, 10665−10675

(88) Ottesen, R. T.; Birke, M.; Finne, T. E.; Gosar, M.; Locutura, J.; Reimann, C.; Tarvainen, T.; Team, G. P. Mercury in European agricultural and grazing land soils. *Appl. Geochem.* **2013**, *33*, 1−12.

DOI: 10.1021/acs.est.9b02386
Environ. Sci. Technol. 2019, 53, 10665−10675